Measurement accuracy in control of segmented-mirror telescopes

Douglas G. MacMartin and Gary Chanan

Design concepts for future large optical telescopes have highly segmented primary mirrors, with the out-of-plane degrees of freedom actively controlled. We estimate the contribution to errors in controlling the primary mirror that results from sensor noise and, in particular, compare mechanical measurements of relative segment motion with optical wave-front information. Data from the Keck telescopes are used to obtain realistic estimates of the achievable noise due to mechanical sensors. On the basis of these estimates, mechanical sensors will be more accurate than wave-front information for any of the telescope design concepts currently under consideration, and therefore supplemental wave-front sensors are not required for real-time figure control. Furthermore, control system errors due to sensor noise will not significantly degrade either seeing-limited or diffraction-limited observations.

OCIS codes: 010.7350, 110.6770, 120.6650.

1. Introduction

Various ground-based optical–infrared telescopes with effective apertures of 30 m or more are currently in the planning stages.[1–4] Most of these design concepts involve a highly segmented primary mirror, with as many as a few thousand segments. The out-of-plane degrees of freedom of each segment must be actively controlled, which requires precise information about the displacement of each segment. The 36-segment primary mirrors of the twin Keck telescopes use capacitive displacement sensors to measure relative motion between neighboring segments,[5,6] and a similar approach is presumed for most future telescopes. With any set of sensors that responds only to relative motion, deflection shapes with high spatial wave number are sensed more accurately than those of low wave number. Optical wave-front information could be used to supplement these sensors to estimate the displacement of the low-spatial-wave-number modes. However, turbulence in the direction of the guide star is uncorrelated with the turbulence over most of the seeing-limited telescope field of view, and thus wave-front information provides a noisy estimate of mirror deformations.[7,8]

The control matrices for relative displacement sensors for large segmented-mirror telescopes have been developed by Chanan *et al.*,[9] from which the noise propagation characteristics have been obtained. In this paper we provide a quantitative assessment of the resulting contribution to both the seeing-limited and the diffraction-limited error budgets of the telescope as a function of the bandwidth of active control. In addition to the error multiplier from Ref. 9, this requires a realistic estimate of the power spectral density (PSD) of the sensor noise, which we obtain using data from the Keck telescopes. The performance of relative displacement sensors can then be compared directly to wave-front information.

The significance of errors resulting from measurement noise needs to be understood in context with reasonable performance targets for two operational modes: seeing-limited [without adaptive optics (AO)] and diffraction-limited (with AO). A reasonable goal for seeing-limited observations is for the telescope to degrade image quality by less than 10%, which we measure by the 80% enclosed-energy image diameter $\theta(80)$. The 90th percentile atmospheric turbulence degraded image size at Mauna Kea is 0.57 arc sec.[1] Thus all telescope sources should contribute $\theta(80) < 0.26$ arc sec, and any one source such as

D. G. MacMartin (macmardg@cds.caltech.edu) is with the Department of Control and Dynamical Systems, California Institute of Technology, Pasadena, California 91125. G. Chanan is with the Department of Physics and Astronomy, University of California, Irvine, Irvine, California 92697.

Received 5 July 2003; revised manuscript received 24 September 2003; accepted 8 October 2003.

0003-6935/04/030608-08$15.00/0

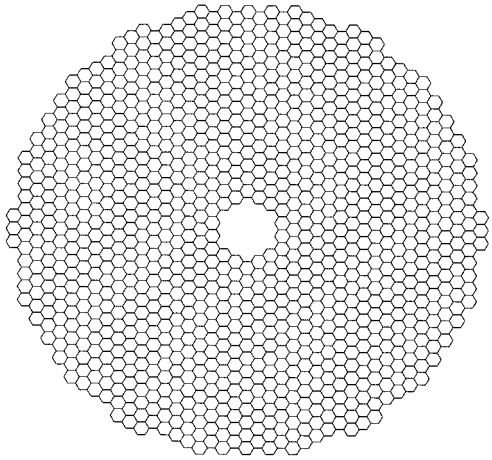

Fig. 1. Segmentation geometry for the CELT 15-m radius primary mirror, with 1080 segments of circumscribed radius $a = 0.5$ m.

sensor noise must be significantly smaller. For diffraction-limited observations, a reasonable target of a Strehl ratio of 0.5 at a wavelength of 1 μm requires the total error from all sources to be less than 133-nm rms. The total uncorrectable wave-front error due to all telescope sources should be of the order of 50-nm rms, with any one source being much smaller. Low-wave-number distortions of the primary mirror can be corrected by the AO system provided that this does not result in saturation of the AO actuators.

In Section 2 we review and generalize the construction of control matrices and resulting error multipliers. In Section 3 we provide an analysis of edge sensor data from Keck. In Sections 4 and 5 we estimate the corresponding contributions to telescope performance for relative displacement sensors and wave-front information, respectively. With only relative displacement sensors, the low-wave-number (spatially smooth) modes have poor observability and thus have larger rms surface errors for a given sensor noise. Nonetheless, sufficient performance can be achieved with feedback that uses only these sensors, whereas wave-front information will have higher sensor noise on any time scale due to atmospheric turbulence. We conclude that use of real-time wave-front information for primary mirror figure control is not necessary, although optical measurements will still be required periodically to determine the desired sensor readings.

For specific numerical estimates, we use parameters from the California Extremely Large Telescope (CELT).[1] The 30-m-diameter CELT primary mirror has 1080 hexagonal segments (as illustrated in Fig. 1), 3240 actuators, and 6204 edge sensors.[10,11]

2. Control Analysis

For the Keck telescopes, three actuators located at the vertices of an equilateral triangle adjust the piston, tip, and tilt of each segment in response to a set of displacement sensor readings.[5,6] There are two

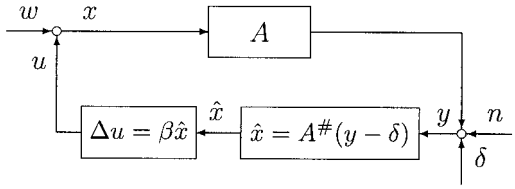

Fig. 2. Control block diagram. For the control, we estimate the displacement $\hat{x}$ from sensors y and use this to determine the desired control command u.

displacement sensors along each intersegment edge, which are sensitive to both the relative out-of-plane displacement between segments and also to the changes in the dihedral angle between segments. A similar control geometry is assumed for future large segmented-mirror telescopes. The edge-mounted displacement sensors redundantly measure all $(3n_{\text{seg}} - 3)$ relative pistons, tips, and tilts of the n_{seg} segments.

The deformation of the primary mirror with respect to the desired shape can be described by the vector x of displacements at each of the actuator locations. The vector of sensor measurements y that results from segment displacements satisfies

$$y = Ax + \delta + n, \tag{1}$$

with zero-mean sensor noise n. The matrix A is determined from the segment geometry and the actuator and sensor locations; see Chanan *et al.*[9] for details. The desired sensor readings δ corresponding to the desired mirror shape are determined optically. If additional sensors are also used (such as wave-front information), then y can be expanded to include both sets of measurements.

The baseline disturbance rejection control algorithm[5,12] can be divided into two steps, shown in Fig. 2. The first step is to estimate the displacements at the actuator locations given the sensor information, and the second step is to use a simple controller to minimize this error.

In the absence of sensor noise the optimal estimator is

$$\hat{x} = A^{\#}(y - \delta), \tag{2}$$

where the left pseudoinverse $(\cdot)^{\#}$ is given by

$$A^{\#} = \lim_{\rho \to 0}(A^T A + \rho I)^{-1} A^T. \tag{3}$$

For simplicity, assume integral control; with gain β the desired change in the actuator commands u is

$$\Delta u = \beta \hat{x}. \tag{4}$$

If the bandwidth is much lower than the sample rate f_s, the control law can be approximated by a continuous-time integrator $u(s) = (k/s)A^{\#}[y(s) - \delta]$, where s is the Laplace variable, $k = f_s\beta$ is the equivalent continuous-time gain, and the bandwidth is $f_c = k/(2\pi)$ in hertz. The response from sensor noise to surface error x is the product of $A^{\#}$ and the low-pass

filter $(1 + s/k)^{-1}$; the filter passes estimation errors due to sensor noise through to surface errors below the control bandwidth and attenuates higher-frequency errors. For white-noise input to this filter with PSD Φ (variance per hertz), the variance of the output of the filter is $(\pi/2) f_c \Phi$.

For specificity, two plausible control bandwidths are considered in the following. The bandwidth sufficient to compensate for gravity and thermal deformations is the same as that in use at Keck of ~0.05 Hz. A higher bandwidth would be required to compensate for wind-induced deformation of the primary mirror.[13] In the absence of accurate models of wind buffeting and the resulting control bandwidth requirements, we assume a 2.5-Hz bandwidth for illustration only. This is likely to be adequate, and achieving a significantly higher control bandwidth for 30-m or larger telescopes may be challenging because of the interaction with structural modes. Extending the analysis to allow for the control bandwidth to vary as a function of spatial frequency is straightforward.

Returning to the estimation problem from Eq. (2), note that the left pseudoinverse is readily computable from the singular-value decomposition $A = U\Sigma V^T$, where Σ is a diagonal matrix of singular values σ_i and U and V are unitary. The deflection shapes corresponding to each column of V are referred to as modes. With only relative measurements, the matrix A has three singular values equal to zero, corresponding to overall rigid-body deflection of the primary mirror. The mode corresponding to zero relative edge displacement between segments and equal dihedral angle between segments is almost pure focus. This mode is observable with sensors sensitive to both dihedral angle and displacement as is true at Keck and with the nominal sensor geometry planned for CELT.[9]

Large singular values of A correspond to highly observable deflection shapes, with large deflections between neighboring segments for a given overall rms deflection. Small singular values correspond to low-spatial-wave-number (smooth) deflection shapes, with relatively less deflection between segments for a given overall deflection; these approximately match the lowest-order Zernike basis functions. Modes with small singular value in A have large singular values ${\sigma_i}^{-1}$ in $A^{\#}$, and hence the control law will amplify whatever sensor noise exists in these directions. Assuming that the noise on different sensors is uncorrelated, the rms error in the estimation of the deflection at the actuator locations is the product of the rms sensor noise and an error multiplier N, given by

$$N^2 = \sum_{i=1}^{n_{\mathrm{act}}} N_i^2 = \sum_{i=1}^{n_{\mathrm{act}}} \frac{{\sigma_i}^{-2}}{n_{\mathrm{act}}}. \tag{5}$$

Values of N for specific segmentation designs are given in Ref. 9. For a general scaling argument, consider fitting a smooth surface (the deviation of the mirror from the desired shape) with rigid flat segments; the resulting gaps at the segment edges are proportional to the sensor output. Flat segments can fit a uniform slope perfectly with zero vertical gaps between segments, but with nonzero curvature in two dimensions, the best fit will have vertical gaps between segments that are proportional to the square of the segment radius a and the second derivative of the displacement shape. Figure 3 shows the vertical gap d_i between a segment corner and a smooth deflection shape for each corner at the intersection of three hexagonal segments. The extra factor of 2 results from our assuming a best rms fit, rather than matching the smooth shape only at the center of each segment. Differencing the gaps across segments gives an estimate of each sensor response. The accuracy with which relative displacement measurements can sense smooth modes with feature sizes much larger than an individual segment is therefore related to the curvature of the displacement shape. For hexagonal segments with intersegment relative displacement sensors exactly at the corners, the (area-averaged) mean-square sensor response over the mirror surface due to a displacement error $f(x, y) = f(r \cos\theta, r \sin\theta)$ is

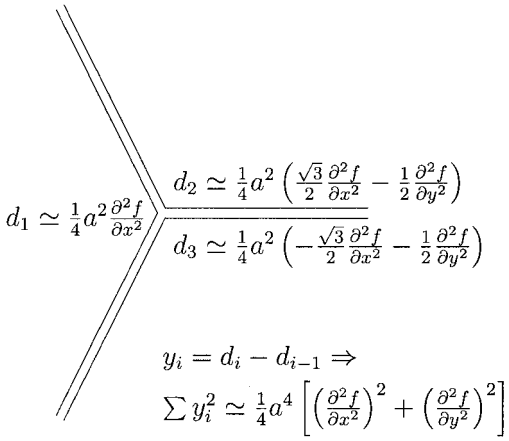

Fig. 3. Detail of a generic estimate of the relative displacement sensor response at the intersection of three hexagonal segments. The vertical gap d_i between a segment corner and a smooth deflection shape is proportional to the segment radius squared and the curvature. The difference between these gaps is measured by relative displacement sensors at the segment corners. The mean-square response of the three sensors at a segment intersection is given by Eq. (6).

$$\Psi(f) = \frac{1}{4\pi}\left(\frac{a}{R}\right)^4 \int_0^1 \int_0^{2\pi} \left[\left(\frac{\partial^2 f}{\partial x^2}\right)^2 + \left(\frac{\partial^2 f}{\partial y^2}\right)^2\right] r\,dr\,d\theta, \tag{6}$$

where the spatial coordinates are normalized by the mirror radius R so that r, x, and y are dimensionless. The number of degrees of freedom of the segment array is $n_{\mathrm{act}} \simeq 3(R/a)^2$. For a mode with displacement f_i scaled to give unit mean-square surface motion, the error multiplier is ${N_i}^2 = [\Psi(f_i) n_{\mathrm{act}}]^{-1}$. The error multiplier N therefore scales with the ratio of mirror radius to segment radius R/a (or to the square

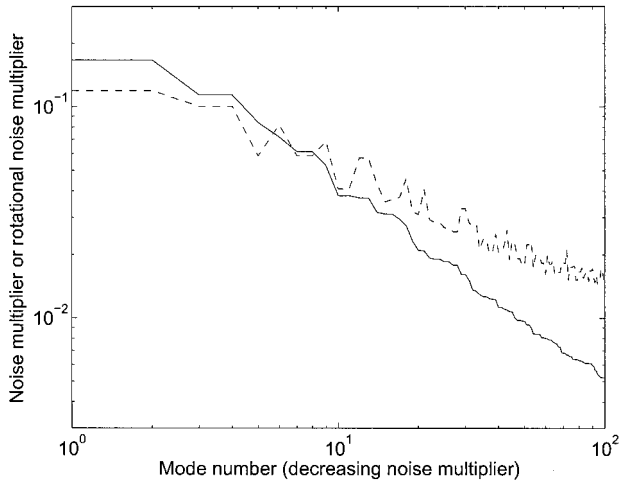

Fig. 4. Theoretical modal error multipliers for relative displacement sensors. The solid curve is the error multiplier N_i from sensor noise to displacement, divided by (R/a) (dimensionless). The dashed curve is the rotational error multiplier $(N_\theta)_i$ from sensor noise to rms segment rotation, divided by $1/a$ (in mas/nm for a in m). Modes are Zernike basis functions sorted by error multiplier.

root of the number of segments). Because the least-observable modes obtained from A correspond to Zernike basis functions, these can be used to estimate the modal and total error multiplier. Excluding focus mode (which involves sensitivity only to the dihedral angle) and computing the integrals numerically for Zernike basis functions yields $N \simeq 0.35R/a$. Alternatively, fitting the results from Ref. 9 for sensors sensitive only to displacement yields a rough approximation of $N \simeq 0.5R/a$. The approximation based on Eq. (6) is thus accurate to within a factor of 2.

For seeing-limited observations, the contribution to image blur depends on rms segment rotation θ_{rms} rather than surface errors. For a Gaussian distribution, $\theta(80) = 1.27 \times 2\theta_{\mathrm{rms}}$. For each mode, compute the geometric multiplier Θ_i as the ratio of mean-square rotation resulting from unit displacement in that mode:

$$\Theta(f) = \frac{1}{\pi R^2} \int_0^1 \int_0^{2\pi} \left[\left(\frac{\partial f}{\partial x} \right)^2 + \left(\frac{\partial f}{\partial y} \right)^2 \right] r \mathrm{d}r \mathrm{d}\theta. \quad (7)$$

The rms surface rotation that results from sensor noise is

$$N_\theta{}^2 = \sum_{i=1}^{n_{\mathrm{act}}} (N_\theta)_i{}^2 = \frac{1}{n_{\mathrm{act}}} \sum_{i=1}^{n_{\mathrm{act}}} \frac{\Theta_i}{\Psi_i}. \quad (8)$$

From the preceding analysis, this rotational error multiplier scales only with the segment radius a and is independent of the mirror diameter. The modal behavior of N_i and the product $(N_\theta)_i$ is shown in Fig. 4 with the analytical estimates from Eqs. (6) and (7). The rotational error multiplier scales inversely with segment size a and is plotted in milliarcseconds (mas) per nanometer, whereas the nondimensional error multiplier N scales with R/a. The modes are Zernike basis functions sorted by the error multiplier; this decreases with increasing radial degree and decreasing azimuthal degree (these trends are consistent with the error multipliers obtained from detailed analysis in Ref. 9). The total error multiplier N is dominated by the lowest-order, smoothest modes, for which the analytical predictions are accurate. However, higher-order modes are more significant for the rotational error multiplier N_θ. For the analytical estimate, the sum over an infinite number of Zernike modes does not converge because of the cumulative contribution from modes with feature sizes smaller than an individual segment, where the approximation clearly breaks down. The sum for a finite number of modes up to radial degree R/a yields $N_\theta(a) \simeq 0.4/a$ in mas/nm for a in meters. For CELT ($a = 0.5$ m), the total rotational error multiplier (for segment tilts, not ray tilts) for relative displacement sensors[9] is 0.93 mas/nm. This is the noise propagation factor from sensor noise to estimation errors in segment rotations, analogous to the error multiplier N from sensor noise to estimation errors in segment displacements.

3. Analysis of Keck Sensor Data

Data collected at the Keck telescopes were analyzed to estimate the achievable noise with capacitive edge sensors. A total of 83 data sets was used in the analysis, 36 from Keck 1 and 47 from Keck 2. All the data were collected between March and June 2001. Sensor readings were recorded at 100 Hz for all 168 sensors, and each data set was 10.24 s long.

The key to interpretation of the Keck data is the separation of physical (segment motion) from unphysical (e.g., electrical noise) sensor responses. There are 168 sensor measurements, and if the motion is constrained to rigid-body motion of the 36 segments of the primary mirror, then there are only 105 degrees of freedom (overall tip, tilt, and piston do not produce any intersegment motion). The sensor set is thus overdetermined.

The sensor measurements result from both physical motion d and sensor noise n, so $y = Ad + \delta + n$ when we use the Keck A matrix. Project this measurement into physical and unphysical subspaces y_p and y_u given by

$$y_p = (AA^{\#})(y - \delta), \quad (9)$$

$$y_u = (I - AA^{\#})(y - \delta). \quad (10)$$

Using the singular value decomposition of $A = U\Sigma V^T$, we obtain

$$AA^{\#} = U \begin{bmatrix} I_{105} & 0 \\ 0 & 0 \end{bmatrix} U^T, \quad (11)$$

$$I - AA^{\#} = U \begin{bmatrix} 0 & 0 \\ 0 & I_{63} \end{bmatrix} U^T. \quad (12)$$

The rank of the transformations used are thus $n_p = 105$ and $n_u = 63$. Denote by $\langle {y_p}^2 \rangle$, $\langle {y_u}^2 \rangle$ the sum of

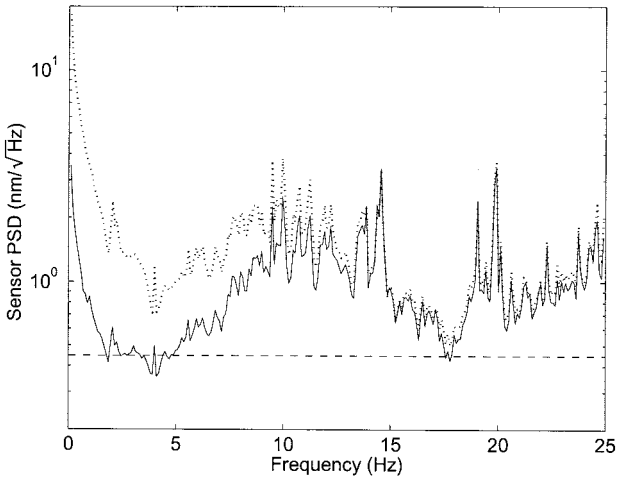

Fig. 5. Average spectrum from Keck 1 displacement sensors, plotted in physical (dotted curve) and unphysical (solid curve) components. The estimated low-frequency noise PSD (see text) is shown by a dotted line.

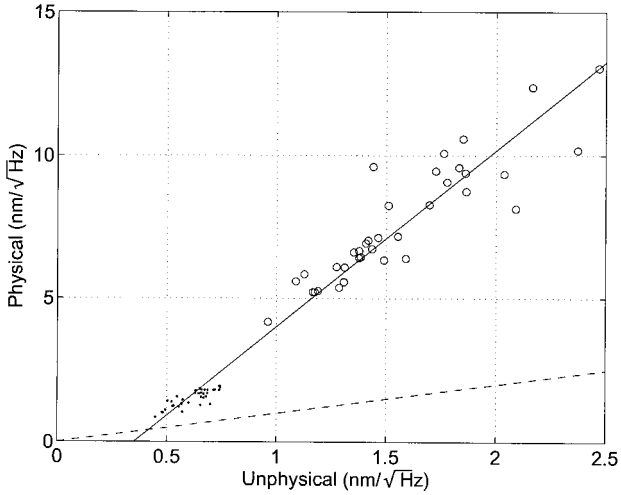

Fig. 6. Low-frequency energy in physical and unphysical directions, Keck 1. Circles are 0–2.5 Hz, dots are 2.5–5 Hz. The dashed line corresponds to equal covariance. The slope of the best-fit line (solid line) is $\alpha^{-1} \sim 6$, and the intercept with $\langle y_p^2 \rangle = \langle y_u^2 \rangle$ is at ~ 0.42 nm/$\sqrt{\text{Hz}}$.

squares normalized by n_p and n_u respectively. If the A matrix used to create these subspaces is exact, then y_u contains information about only the sensor noise n, whereas y_p is influenced by both physical motion and sensor noise. If n is uncorrelated between sensors, then the contribution of sensor noise in y_p can be estimated from the noise in y_u: We have $\langle y_u^2 \rangle = \sigma_n^2$, and $\langle y_p^2 \rangle = \sigma_n^2 + \langle (Ad)^2 \rangle$. If the sensor noise is correlated, then this result is not true; e.g., if there is a component of sensor noise that is correlated across all sensors, then this will show up in y_p (as focus) but not in y_u.

If the A matrix used in the transformation does not match the true A matrix exactly—because, for example, of calibration or fabrication errors—then some true physical motion will result in apparent unphysical sensor readings. It follows that $\langle y_u^2 \rangle = \sigma_n^2 + \alpha \langle (Ad)^2 \rangle$ for some constant α that is a function only of the errors in the A matrix. The transformation is sensitive to small errors; on the basis of a large number of simulations, a 1% random error in each nonzero element of the Keck A matrix yields $\alpha \sim 0.2$. If the statistics of the noise can be assumed to remain constant while the physical disturbances change, then we can obtain the noise statistics by plotting $\langle y_p^2 \rangle$ against $\langle y_u^2 \rangle$. Low-frequency vibrations change considerably between data sets at Keck, and therefore this approach can be used to estimate the noise statistics.

The spectra of y_p and y_u were computed, averaged over sensors with n_p and n_u used for normalization, and averaged over data sets for both Keck 1 and Keck 2. The results are plotted in Fig. 5 for Keck 1; the data for Keck 2 are similar, with slightly higher levels of both physical and unphysical responses. Over much of the frequency range, the physical and unphysical components are comparable, indicating that most of the energy in the sensor signals is due to uncorrelated noise. However, the physical component exceeds the unphysical at low frequencies (and also from 25 to 45 Hz). Although much of the spectrum is relatively constant from data set to data set, the amplitude of the low-frequency component below 10 Hz varies considerably between data sets. One plausible hypothesis is that this component results from wind-induced deformations of the telescope structure. The average over these data sets of the estimated residual surface error at Keck due to uncontrolled low-frequency vibration is 50–75 nm.[14]

The low-frequency spectrum is of primary interest for assessment of control system noise, and the sensor noise level is estimated with the approach outlined above. Figure 6 shows the correlation between the low-frequency energy in the physical and unphysical components for Keck 1, averaged over 0–2.5 Hz and from 2.5 to 5 Hz. Pure sensor noise should result in $\langle y_p^2 \rangle = \langle y_u^2 \rangle$, shown in the plot as a dashed line. Assuming that the observed correlation between the computed physical and the unphysical response is a result of our using an inexact A matrix to transform the motion, we conclude that the true sensor noise is the intercept where $\langle y_p^2 \rangle = \langle y_u^2 \rangle$, given by a mean-square noise of 0.2 nm^2/Hz. The increase above this noise level in the unphysical direction for many of the data sets is simply the result of an inaccurate transformation from sensor measurements to physical and unphysical coordinates (corresponding to errors of less than 1% between the actual and the assumed A matrices). A similar plot can be generated for Keck 2: The apparent noise level below 5 Hz is roughly 0.2 nm^2/Hz for most data sets; however, some of the data sets appear to indicate higher noise levels on Keck 2. Although future telescopes may have a different sensor geometry from Keck, it is reasonable to presume that similar noise performance can be obtained. To be conservative, the re-

mainder of the analysis is conducted with 1 nm^2/Hz, more than double the expected rms noise level.

4. Errors from Relative Displacement Sensors

A. Surface Displacement Errors

The variance of the surface errors that result from sensor noise can be computed as the product of the error multiplier squared N^2, the estimated sensor covariance Φ, and the filtering due to the control bandwidth $(\pi/2)f_c$. The first factor depends on the details of the sensor geometry and placement and scales with the ratio of mirror-to-segment diameter.

Note that focus mode differs from higher-order modes in that this error can be compensated by motion of the secondary, with a residual error due to scalloping.[1] The contribution from focus mode thus depends on both the control bandwidth of the primary mirror and that of the secondary. In the current analysis, we ignore the reduction in error that could thus be achieved. With a deformable secondary mirror, similar corrections could be applied for higher-order modes as well.

Using the approximation obtained above for N, we obtain the rms surface error resulting from sensor noise:

$$\langle \sigma_x^{\,2} \rangle^{1/2} = 0.35 \left(\frac{R}{a} \right) \left(\Phi \, \frac{\pi}{2} f_c \right)^{1/2}. \tag{13}$$

For $R = 15$ m, $a = 0.5$ m, $\Phi = 1$ nm^2/Hz, and $f_c = 0.05$ Hz or $f_c = 2.5$ Hz, $\langle \sigma_x^{\,2} \rangle^{1/2} = 3$ or 20 nm rms.

B. Seeing-Limited Errors

The relevant metric for seeing-limited observations is the mean-square image blur that results from sensor noise, which we quantify in terms of the 80% enclosed-energy image diameter $\theta(80)$. This can be estimated as the product of the rotational error multiplier N_θ, the rms sensor noise, the control bandwidth term, and the conversion factor from segment tips and tilts to $\theta(80)$ of 2×1.27:

$$\theta(80) = 2.54 \left(\frac{0.4}{a} \, \frac{\text{mas}}{\text{nm}} \right) \left(\Phi \, \frac{\pi}{2} f_c \right)^{1/2}. \tag{14}$$

For $a = 0.5$ m and $\Phi = 1$ nm^2/Hz, the contribution to $\theta(80)$ from relative displacement sensors for control bandwidths of $f_c = 0.05$ Hz or $f_c = 2.5$ Hz is <1 mas or 5 mas, respectively. In either case, this is small compared to the target for telescope errors unless much smaller segments are proposed, a much higher control bandwidth is used, or a much larger sensor noise is encountered than that at Keck.

C. Diffraction-Limited Errors

With AO on, most of the errors introduced by sensor noise can be corrected. The errors that remain result largely from edge discontinuities between segments. We can obtain a rough estimate for these errors by noting that each intersegment edge has two edge sensors, so that the resulting uncertainty in the edge discontinuity is $1/\sqrt{2}$ times the individual sensor noise.

The fraction of the rms edge discontinuity remaining after correction by AO is approximated by a two-dimensional geometric argument. If the deformable mirror slopes are piecewise constant, then the residual displacement can be obtained from the ratio $\eta = l/a$, where l is the apparent spacing between deformable mirror actuators as seen at the segmented mirror and a is the segment radius. The best fit to a segment edge discontinuity σ_{edge} yields a nonzero residual error as a function of the distance x from the segment edge of $z(x) = \pm(1/2 - |x|/l)\sigma_{\text{edge}}$ for $|x| \leq l/2$. Integrating $z^2(x)$ over the length of a segment gives the AO-controlled rms surface error σ_{ctrl} in terms of the primary mirror rms edge discontinuity σ_{edge} as $\sigma_{\text{ctrl}} = (\eta/24)^{1/2}\sigma_{\text{edge}}$. For a deformable mirror with $\sim$7000 actuators and a primary mirror with 1080 segments, $\eta \sim 0.8$, hence $\sigma_{\text{ctrl}} \simeq 0.18\sigma_{\text{edge}}$.

The residual wave-front error resulting from sensor noise propagation is therefore given by the product of all these factors:

$$\sigma_{\text{wf}} = 2 \left(\frac{\eta}{24} \right)^{1/2} \left(\frac{1}{\sqrt{2}} \right) \left(\Phi \, \frac{\pi}{2} f_c \right)^{1/2}. \tag{15}$$

For $\eta = 0.8$ and $\Phi = 1$ nm^2/Hz, the contribution to wave-front error from relative displacement sensors for control bandwidths of $f_c = 0.05$ Hz or $f_c = 2.5$ Hz will be <0.1 nm or $\sim$0.5 nm, respectively. Thus, as with seeing-limited observations, measurement noise from relative displacement sensors will not affect diffraction-limited observations unless either much higher control bandwidth is used or much larger sensor noise is encountered than that at Keck.

5. Inclusion of Wave-Front Information

The analysis above suggests that, for future telescope designs currently being considered, sensors that measure the relative displacement between segments can be expected to provide sufficiently accurate displacement estimates for the lowest-order modes. Furthermore, this conclusion also holds if either the sensor noise or the required control bandwidth are increased substantially. Nonetheless, an estimate of the errors associated with the use of wave-front information to estimate the displacement of the low-wave-number modes is relevant.

With AO on, wave-front information is already being used in the control loop. The lowest-frequency content of the AO deformable mirror corrections could be off-loaded to the primary mirror if desired. The need for supplemental wave-front information must therefore be asked in the context of seeing-limited observations only.

For seeing-limited observations, the desired field of view is much larger than the isoplanatic angle over which the atmospheric turbulence can be considered correlated. Therefore turbulence in the direction of the guide star used to provide information is noise on the intended measurement of the primary mirror

shape. This is the dominant source of sensor noise; photon and read noise can be neglected.

Padin[7] has estimated the contribution from atmospheric turbulence to sensor noise as a function of Zernike radial degree n and integration time. By use of a von Karman spectrum to account for the outer scale L_0 in the atmospheric turbulence, the temporal spectrum with frequency f normalized by the mirror radius and turbulent layer velocity v is given by[7]

$$F_n\left(\frac{fR}{v}\right) = 0.023\left(\frac{R}{r_0}\right)^{5/3}\frac{n+1}{\pi^2} \times \int_{-\infty}^{\infty}\frac{J_{n+1}(2\pi\mu)^2}{\mu^2[\mu^2 + (R/L_0)]^{11/6}}\,\mathrm{d}k, \quad (16)$$

where $\mu^2 = k^2 + (fR/v)^2$. For a given control bandwidth f_c, the resulting variance on a mode of radial degree n is

$$\langle\sigma^2(f_c, n)\rangle = \int_0^{\infty}\frac{1}{1 + (f/f_c)^2}F_n\left(\frac{fR}{v}\right)\mathrm{d}f. \quad (17)$$

To obtain a quantifiable comparison with relative displacement sensors, consider primary mirror radius $R = 15$ m, wavelength $\lambda = 0.55$ μm, seeing $r_0 = 0.2$ m, outer scale $L_0 = 2R$, and turbulent layer wind speed $v = 10$ m/s. Note that either larger measurement wavelength λ or larger outer scale L_0 will result in larger atmospheric turbulence and hence worse performance. With these parameters, the total atmospheric wave-front error is of the order of 800 nm, with 185 nm in each $n = 2$ mode (focus and two astigmatism modes). For the control bandwidths considered of 0.05 or 2.5 Hz, the residual atmospheric phase in each $n = 2$ mode on time scales long enough to affect the measurement is 70- and 184-nm rms, respectively. For comparison, the corresponding errors resulting from relative displacement sensors for $n = 2$ obtained by use of the parameters from CELT ($R = 15$ m, $a = 0.5$ m) are 1- and 8-nm rms, respectively. The resulting closed-loop displacement error due to measurement noise for each Zernike mode is shown in Fig. 7 for both atmospheric turbulence corrupted wave-front information and for relative displacement sensors with noise characteristics similar to those of the Keck sensors.

Although wave-front information will be periodically required to establish the desired sensor readings δ, it will not be useful for real-time control unless the internal sensors are significantly worse than expected, or the number of segments is increased significantly (increasing the error multiplier for A).

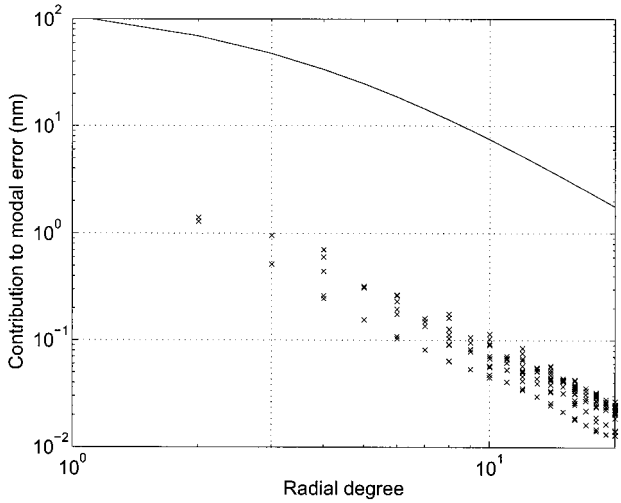

Fig. 7. Closed-loop rms displacement error in nanometers due to measurement noise as a function of the Zernike radial degree for atmospheric turbulence corrupted wave-front information (upper curve, $\lambda = 0.55$ μm, $r_0 = 0.2$ m, $L_0 = 2R = 30$ m) and relative displacement sensors (crosses, $R = 15$ m, $a = 0.5$ m). A control bandwidth of 0.05 Hz was assumed; higher control bandwidth results in higher errors from either sensor set.

6. Conclusions

Future extremely large telescopes with highly segmented primary mirrors require active control to maintain the figure of the primary in the presence of disturbances. As the number of segments increases, there is a decrease in the accuracy of the estimation of low-wave-number (smooth) errors in the primary mirror when only relative measurements are used. The error multiplier that relates estimation errors to measurement noise is a function of the sensor–actuator influence matrix, but can be estimated from the curvature of the basis functions used to represent the mirror deflection shape; the contributions to image blur can similarly be estimated with the slope of the basis functions.

A detailed analysis of data collected at Keck Observatory suggests that the relative displacement sensors in use there have less than 1-nm^2/Hz noise. This is considerably lower than previous estimates, which did not distinguish sensor noise from low-frequency segment vibration. The actuator position errors that result from sensor noise are a product of two factors: the error multiplier discussed above and the sensor noise filtered by the control bandwidth. The resulting wave-front error is primarily in the lowest-wave-number, spatially smooth modes. The contributions to the error budget for seeing-limited observations are estimated from the rms segment tip and tilt that results from sensor noise. For diffraction-limited observations, it is assumed that the deformable mirror can correct spatially smooth errors, and only intersegment edge discontinuities are relevant.

For specificity, the resulting errors are estimated for the parameters of the CELT, where the mirror radius is $R = 15$ m and the segment size is $a = 0.5$ m. For a control bandwidth of 2.5 Hz, we expect a contribution to seeing-limited image diameter due to relative displacement sensors of $\theta(80) \sim 5$ mas and a contribution to uncorrectable rms wave-front error of <1 nm for diffraction-limited observations. We therefore conclude that control system errors due to

displacement sensor noise are not a problem for 30-m class telescopes. This conclusion is dependent on the assumption that the sensor noise is not significantly worse than that found at Keck, and for reasonable control bandwidths. Furthermore, for observations over the seeing-limited field of view of the telescope, atmospheric turbulence is uncorrelated and thus acts as measurement noise in the estimation of the deflections of a segmented mirror. On the basis of optimistic estimates of this contribution, relative displacement sensors will be more accurate than wave-front information on any time scale. As a result, wave-front information is not required for real-time control of relative displacement within the segmented mirror, but only for the establishment of the desired sensor readings.

References

1. J. Nelson and T. Mast, eds., "Conceptual design for a 30-meter telescope," CELT Rep. 34 (California Institute of Technology, Pasadena, Calif., and University of California, Irvine, Calif., 2002), available at http://celt.ucolick.org.
2. S. E. Strom, L. Stepp, and B. Gregory, "Giant Segmented Mirror Telescope: a point design based on science drivers," in *Future Giant Telescopes*, R. Angel and R. Gilmozzi, eds., Proc. SPIE **4840,** 116–128 (2002).
3. T. Andersen, A. Ardeberg, J. Beckers, A. Goncharov, M. Owner-Petersen, H. Riewaldt, R. Snel, and D. Walker, "The Euro50 Extremely Large Telescope," in *Future Giant Telescopes*, R. Angel and R. Gilmozzi, eds., Proc. SPIE **4840,** 214–225 (2002).
4. P. Dierickx, B. Delabre, and L. Noethe, "OWL optical design, active optics, and error budget," in *Optical Design, Materials, Fabrication, and Maintenance*, P. Dierickx, ed., Proc. SPIE **4003,** 203–211 (2000).
5. R. C. Jared, A. A. Arthur, S. Andreae, A. Biocca, R. W. Cohen, J. M. Fuertes, J. Franck, G. Gabor, J. Llacer, T. Mast, J. Meng, T. Merrick, R. Minor, J. Nelson, M. Orayani, P. Salz, B. Schaefer, and C. Witebsky, "The W. M. Keck Telescope segmented primary mirror active control system," in *Advanced Technology Optical Telescopes IV*, L. D. Barr, ed., Proc. SPIE **1236,** 996–1008 (1990).
6. R. Cohen, T. Mast, and J. Nelson, "Performance of the W.M. Keck telescope active mirror control system," in *Advanced Technology Optical Telescopes V*, L. M. Stepp, ed., Proc. SPIE **2199,** 105–116 (1994).
7. S. Padin, "Wind-induced deformations in a segmented mirror," Appl. Opt. **41,** 2381–2389 (2002).
8. R. N. Wilson and L. Noethe, "Closed-loop active optics: its advantages and limitations for correction of wind-buffet deformations of large flexible mirrors," in *Active Telescope Systems*, F. J. Roddier, ed., Proc. SPIE **1114,** 290–301 (1989).
9. G. Chanan, D. G. MacMartin, J. Nelson, and T. Mast, "Control and alignment of segmented-mirror telescopes: matrices, modes, and error propagation," Appl. Opt. (to be published).
10. T. Mast and J. Nelson, "Segmented mirror control system hardware for CELT," in *Optical Design, Materials, Fabrication, and Maintenance*, P. Dierickx, ed., Proc. SPIE **4003,** 226–240 (2000).
11. D. G. MacMartin, "Control challenges for extremely large telescopes," in *Smart Structures and Materials 2003: Industrial and Commercial Applications of Smart Structures Technology*, E. H. Anderson, ed., Proc. SPIE **5054,** 275–286 (2003).
12. D. G. MacMartin, T. S. Mast, G. Chanan, and J. E. Nelson, "Active control issues for the California Extremely Large Telescope," paper AIAA-2001-4035, presented at the Guidance, Navigation, and Control Conference, Montreal, Canada, 6–9 August 2001 (American Institute of Aeronautics and Astronautics, Reston, Va., 2001).
13. S. Padin and W. Davison, "Model of image degradation due to wind buffeting on an extremely large telescope," Appl. Opt. **42,** 592–600 (2004).
14. D. G. MacMartin and G. Chanan, "Control of the California Extremely Large Telescope Primary Mirror," in *Future Giant Telescopes*, R. Angel and R. Gilmozzi, eds., Proc. SPIE **4840,** 69–80 (2002).